International Journal of Mechanical and Production Engineering Research and Development (IJMPERD)
ISSN (P): 2249–6890; ISSN (E): 2249–8001
Vol. 9, Issue 6, Dec 2019, 735–746

SUPERSONIC FLOW OVER A CYLINDRICAL PROTRUSION WITH VORTEX GENERATOR

P. S. VIGNESH RAM[1] & KIM HEUY DONG[2]

[1]*Research Scholar, Department of Mechanical Engineering, Andong National University, Andong, South Korea*

[2]*Professor, Department of Mechanical Engineering, Andong National University, Andong, South Korea*

ABSTRACT

Supersonic flow around the cylindrical protrusion can cause a bow shock, which interacts with the incoming flow boundary layer. Such shock wave - boundary layer interaction can lead to a complex flow phenomenon, which increase the aerodynamic drag and also causes the flow unsteadiness. It is essentially more important to reduce the drag and flow unsteadiness by approaching a control technique against the interaction between the shock wave induced by a protrusion and wall boundary layer. In the present work, the control of shock wave boundary layer interaction by a ramp type vortex generator is investigated using unsteady RANS methodology. Vortex generator was placed ahead of cylindrical protrusion into the supersonic stream of Mach number 2.0. The flow fields around the cylindrical protrusion from the present numerical results are compared with the experimental result for steady pressure data. Adopting vortex generator can helps in reduction of surface pressure fluctuation. The frequency spectra for the cylindrical protrusion with vortex generator showed greatly reduced spectral density values, and collapse faster than the case without vortex generator.

KEYWORDS: SWBLI, Vortex Generator, Cylindrical Protrusion & Control

Received: Sep 15, 2019; **Accepted:** Oct 05, 2019; **Published:** Nov 18, 2019; **Paper Id.:** IJMPERDDEC201962

Original Article

1. INTRODUCTION

Shock wave boundary layer interactions (SWBLI) have been a main consent for the past several decades. The effect of such interactions includes the surface heat transfer rate and the high-pressure loads. The necessity of any aerospace vehicle is a smooth and streamlined surface, but due to manufacturing constrain it will always consist of protruded objects like rivets, sheet metal joints, pitot probes, etc. At supersonic speed, these protruded obstacles will encounter a bow shock, which interacts with the incoming boundary layer leads to SWBLI. This causes the incoming boundary layer to separate ahead of the protrusion results in a complex flow phenomenon. The flow field disturbances caused by these protrusions mainly depends on several parameters like free stream Mach number, the height of protrusion and incoming boundary layer thickness [1, 2]. The viscous interactions are more dominated by certain critical areas like pylon mount, wing-body junction and causes high local heating [3] and also several vortices, emerging from the upstream region of cylindrical protrusion causing the disturbance in the flow field, far downstream as counter rotating stream-wise vortices [4, 5].

Most of the early researches are concerned about the separation distance ahead of the protrusion. Sykes [6] investigated flow past finite length cylinder and revealed that the flow field in the root region will be independent when the length to diameter ratio exceed 4, and also drag coefficient for infinite cylinder is around 1.40 at Mach number 2.0. Using optical surface indicator method, Sydney [7] discussed various shapes and size of protrusion immersed into the boundary layer and proposed a correlation for separation distance in terms of height to diameter

ratio. Mashburn [8] conducted numerous experiments on cylindrical protrusion from a small to a large height protrusion with different Mach number in a turbulent flow field. There is a limit for the size of protrusion, where the boundary layer separation is no longer induced and to induce separation minimum of 0.125 inch is necessary. The separation zone and the primary separation line are also depending on stream boundary layer thickness (δ). Verma and Gupta [9] developed a correlation for the separation distance in terms of height, diameter and boundary layer thickness. Like the skin friction coefficient, the aerodynamic heating around the protrusion due to SWBLI was reported by several authors [10, 11]. Many researchers have carried out vast experiments and computational studies related to the surface protrusion height of the order of boundary layer thickness. Li et al.[12] have been performed an experimental study on two types short protuberances, taking the height of the order of turbulent boundary layer thickness and explained, the presence of 3D complex flow field is due to non-homogeneous pressure distribution ahead of the leading edge of the protrusion. Hahn and Frendi [13] have been conducted extensive numerical studies on two different heights of cylindrical protrusion at Mach number 1.6.He describes that the interaction of three-dimensional protrusions with a supersonic turbulent boundary layer causes an increase in sound pressure level with an increase in protrusion height. Shock wave boundary layer interaction due to cylindrical protrusion shows the fluctuation in the size of the separated flow is larger in laminar-like interaction than the turbulent interaction [14]. However, there is vast available literature on the infinite height of protrusion or in the order of incoming boundary layer thickness, and whereas limited to control of unsteady aerodynamics, due to shock wave boundary layer interaction around the small height protrusions.

There are several control techniques in use for reducing the effect of shockwave boundary layer interaction. Conventional boundary layer bleed is one of the techniques to control the separation due to shock wave boundary layer interaction within the supersonic engine inlets. The bleed system has a disadvantage of loss in mass flow rate and low efficiency. For the past decades, researchers found that the passive devices like vortex generators are shown more efficient than the active boundary layer bleed or blowing system. There are different kinds of Vortex Generator (VG) are in use. Traditional vortex generators are usually for control of separation of boundary layer or delay the separation. In supersonic flows, these VG heights are taken equal or less than boundary layer thickness. It can energize the boundary layer by introducing stream-wise vortices into the flow field [15]. Though the VG is also a kind of protrusion or obstacle in the flow field, but it has an advantage of delaying the boundary layer separation and helps in control of SWBLI. Traditional VG has a drag penalty due to its size but smaller VGs of the order of boundary layer thickness can have a minimum drag [16, 17]. Micro VGs are specially used ahead of the flow where it tends to separate. It has the ability to change near-wall boundary layer parameters and more stable to unsteady separation [18, 19]. VGs has a strong influence on the reduction of boundary layer shape factor and making it more robust and less susceptible to the separation, and also several multiple pairs of counter-rotating vortices emerges, which enhance the low momentum fluid near the wall by entraining the outer high momentum fluid [20, 21]. Anderson et al.[22] have been studied control of SWBLI using microarray VG. He optimized the position and shape to study the changes in boundary layer characteristics downstream of SWBLI and explains that its behavior is very similar to conventional inlet boundary layer bleed system and overcome the disadvantages like a loss is a mass flow and pressure loss. The boundary layer displacement thickness is larger downstream of the interaction, leaving us to re-design of inlet geometry by enlarging internal flow passage. The optimization of VG using surface response methodology by considering boundary layer thickness and incompressible shape factor shows VG with less height cause mixing high and low momentum within the boundary layer, whereas the larger VG with strong vortices pulls more fluid towards the wall which shows more benefit. This will help in improving the incompressible shape factor [23, 24]. Using

the vortex generator, upstream of normal shock can lead to 84% of the reduction in separation area downstream. Placing VG downstream of normal shock yields pressure recovery and mass flow ratio of up to 25% and 10%, respectively [25, 26]. In comparison with wedge type sub-boundary layer VG, the counter rotating vane type sub-boundary layer VG shows more effective in alleviating the shock induced separation [27]. The array of backward facing micro VG can only reduce separation directly behind the VG and in between is less effective, whereas placing the second row can improve the health of the boundary layer but separation region was not eliminated [28]. The shockwave boundary layer interaction can also happen by compression ramp, which are predominantly 2 dimensional in nature. But wall mounted protrusion will lead to 3-dimensional effect in the flow field. Using VG ahead of compression ramp can reduce the fluctuating pressure loads in shock wave boundary layer interaction [29]. Control of SWBLI due to cylindrical protrusion has been attempted by Pierce et al. [30] using colored oil flow visualization, but detailed study has not been carried out.

In the present study, an attempt has been made to understand the effect of VG on the flow unsteadiness caused by the cylindrical protrusion at supersonic Mach number 2.0. The effect of VG on aerodynamic drag acting on the cylindrical protrusion is also investigated.

2. COMPUTATIONAL METHODOLOGY

In the present numerical simulation, the compressible ax is ymmetric form of the fluid flow conservation equations is considered. Favre-averaged Navier-Stokes equations for the conservation of mass, momentum and energy and two transport equations for turbulent kinetic energy and specific dissipation rate are solved. The governing equations in the tensor notations are as follows,

$$\frac{\partial \rho}{\partial t}+\frac{\partial}{\partial x_i}\left(\rho u_i\right)=0 \tag{1}$$

$$\frac{D\left(\rho u_i\right)}{Dt}=-\frac{\partial p}{\partial x_i}+\frac{\partial}{\partial x_j}\left[\mu_{eff}\left(\frac{\partial u_i}{\partial x_j}+\frac{\partial u_j}{\partial x_i}-\frac{2}{3}\delta_{ij}\frac{\partial u_k}{\partial x_k}\right)\right]+\frac{\partial}{\partial x_j}\left(-\rho\overline{u_i'u_j'}\right) \tag{2}$$

$$\frac{\partial}{\partial t}\left(\rho E\right)+\frac{\partial}{\partial x_i}\left[u_i\left(\rho E+p\right)\right]=\frac{\partial}{\partial x_i}\left[\left(\alpha+\frac{C_p\mu_t}{P_{rt}}\right)\frac{\partial T}{\partial x_i}+u_j\left(\tau_{ij}\right)_{eff}\right] \tag{3}$$

where, E and T are the mass-averaged values and (τ_{ij}) is the stress tensor, which is due to dissipation and defined as:

$$\tau_{ij}=\mu_{eff}\left[\left(\frac{\partial u_j}{\partial x_i}+\frac{\partial u_i}{\partial x_j}\right)-\frac{2}{3}\left(\frac{\partial u_i}{\partial x_i}\delta_{ij}\right)\right] \tag{4}$$

The equation of state for perfect gases is added to close the system:

$$p=\rho RT \tag{5}$$

In the present work, standard k-ω turbulence model is used. The transport equation for turbulence kinetic energy (k) and the specific dissipation rate (ω) are as follows,

$$\frac{\partial}{\partial t}\left(\rho k\right)+\frac{\partial}{\partial x_i}\left(\rho k u_i\right)=\frac{\partial}{\partial x_j}\left[\left(\mu+\frac{\mu_t}{\sigma_k}\right)\frac{\partial k}{\partial x_j}\right]+G_k-\Delta_k \tag{6}$$

$$\frac{\partial}{\partial t}(\rho\omega)+\frac{\partial}{\partial x_i}(\rho\omega u_i)=\frac{\partial}{\partial x_j}\left[\left(\mu+\frac{\mu_t}{\sigma_k}\right)\frac{\partial\omega}{\partial x_j}\right]+G_\omega-\Delta_\omega \tag{7}$$

where, G_k represents the generation of turbulence kinetic energy due to mean velocity gradients. G_ω represents the generation of ω. Δ_k and Δ_ω represent the dissipation of k and ω due to turbulence, respectively. σ_k and σ_ω are the turbulent Prandtl numbers for k and ω, respectively. The turbulent viscosity μ_t is computed by combining k and ω as follows.

$$\mu_t=\alpha^*\frac{\rho k}{\omega} \tag{8}$$

Compressible 3-Dimensional numerical simulations using unsteady RANS were carried out in the present study. The initial RANS mean flow solution is obtained from two equation (*k*-ω) standard turbulence model, which is then used to initialize the unsteady simulation. The present numerical simulation has been performed using commercial CFD code ANSYS Fluent. The 3D multi-block structured grid was created around the cylindrical protrusion with VG using ICEM CFD. The Advection Upstream Splitting Method (AUSM) was used for solving a governing equation with second order accuracy. Ideal gas was taken as working fluid and viscosity is calculated using Sutherland's viscosity law. For better convergence and stability at the initial stage, the courant number and relaxation factor was initialized with 0.3 and 0.25, respectively. Later, these values are increased gradually to a value of 2 and 0.8 for smooth convergence. The residuals for each conserved variables have reduced below 10^{-6} and simultaneously mass flow rate and drag coefficient value is also monitored to check the solution convergence. For unsteady simulation, the time step is one of the important factors.

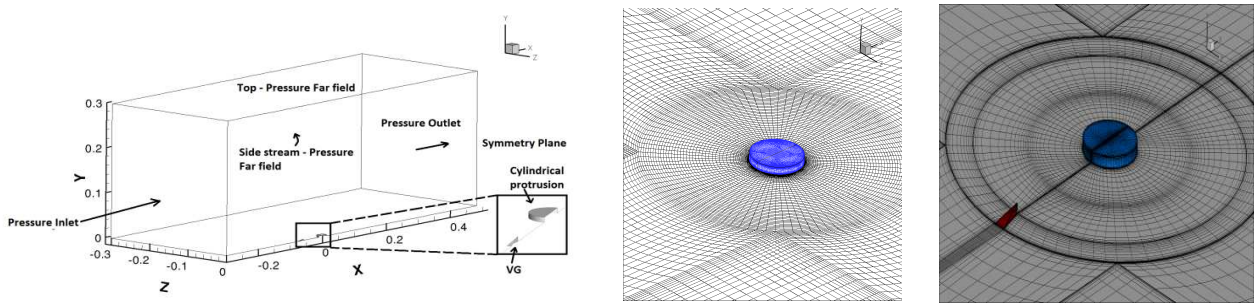

(a) **(b)** **(c)**

Figure 1: (a) Computational Domain along with Boundary Condition, (b) Grid without VG (c) Grid with VG.

Time step taken in the present study is 1 x 10^{-5}s, which is optimized after performing different time steps of 1 x 10^{-3}s and 1 x 10^{-4}s. Though 1 x 10^{-4} s can provide qualitative results for cylindrical protrusion alone, but not able to resolve for cylindrical protrusion with VG and for further reducing the time steps size less than 10^{-5} will increasing the computing time. The unsteady RANS calculation was run for up to 8 x 10^5 time steps corresponding to 0.8s, where first 30000 time steps were allowed to run to get statistically steady solution prior to collect 50000 sampling data for spectral analysis. All the numerical simulation were carried out on a high-performance workstation consists of dual hexa-core Intel Xeon processors at 2.4Ghz with 4GB RAM per core and NVIDIA Quadro K4200. Each case runtime corresponds to an average wall clock time of 25 days. Fluctuating pressure data are monitored at several locations upstream, downstream and on the cylindrical protrusion and drag force acting on cylindrical protrusion is also monitored at each time step. The flow parameters are taken for the present simulations are Mach number 2.0 and a Reynolds number per meter of 3.8 x 10^6. The coefficient of pressure obtained from steady simulation is compared with the experimental data [24]. The height of protrusion (H_C) and diameter (D) are 3mm and 24mm. The boundary layer thickness δ is 3mm maintained same as an

experimental condition. A triangular ramp type VG is used in the present study to control SWBLI. The height of vortex generator H_{vg} is 3 mm; the ramp angle is 12 deg and chord length is 12 mm. The computational domain along with the boundary conditions adopted in the present study is shown in figure 1(a). The length, width, and height of overall computational domain are 35D, 12.5D and 12.5 D respectively. Although the VG model is simple, the grid around its surrounding volume can be challenging one especially hexahedral grid. Due to its triangular shape and sharp corners can lead to highly skewed cells in the vicinity of VG. In the present work, the hexahedral grid around the VG was made using structured block methodology. The grid around the cylindrical protrusion and cylindrical protrusion with VG is shown in figure 1(b and c). The first cell size of the grid near the wall is taken as 10^{-3} mm corresponding to wall Y^+ = 0.83. The overall cell count in the flow domain for only cylinder model and for cylinder model with VG is 2 and 2.3 million cells respectively.

3. RESULTS AND DISCUSSIONS

In the present numerical study, a cylindrical protrusion with height (H_C) 3 mm and diameter (D) is 24 mm at Mach number is simulated. The supersonic flow around the cylindrical protrusion cause upstream bow shock, which interacts with the incoming boundary layer leads to a lambda shock structure and tends to separate the boundary layer. This separation distance depends on the protrusion height (H_C), and free stream Mach number. It has been shown that increasing the protrusion height will result in increasing the separation distance and the upstream stagnation pressure [23, 24].

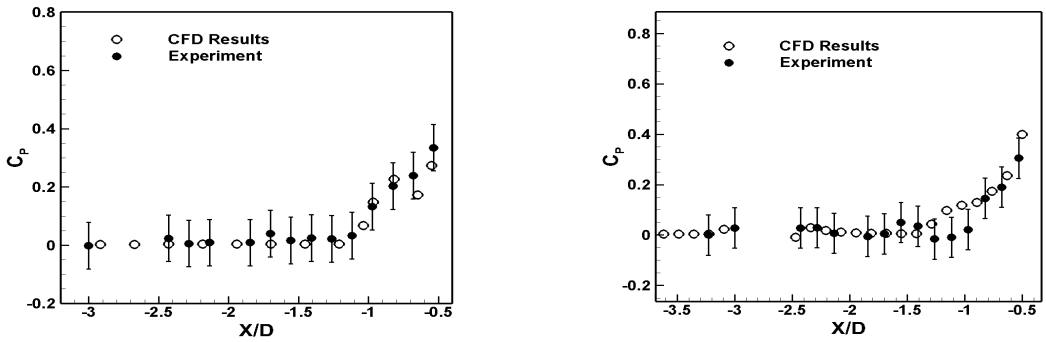

(a) Without VG **(b) with VG**

Figure 2: Comparison of CFD Results to Experimental Data [25] for C_p.

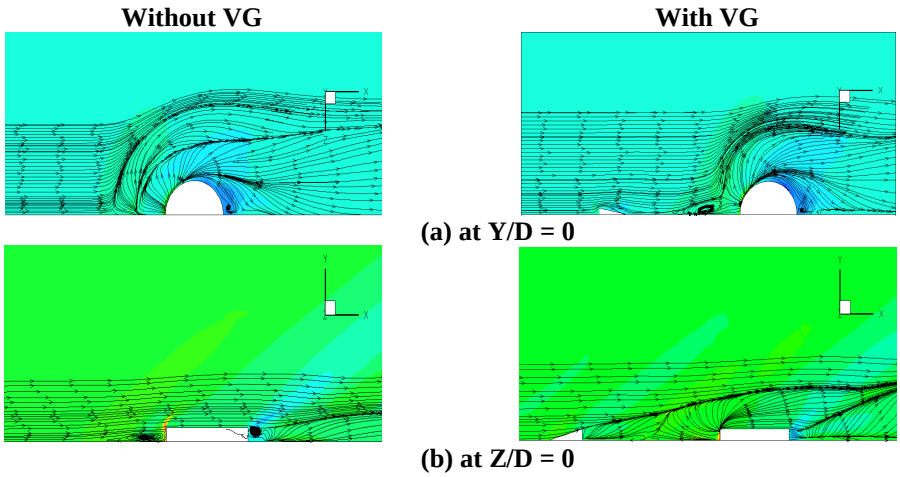

(a) at Y/D = 0

(b) at Z/D = 0

Figure 3: Streamline Pattern with and without Vortex Generator at Mach Number 2.0.

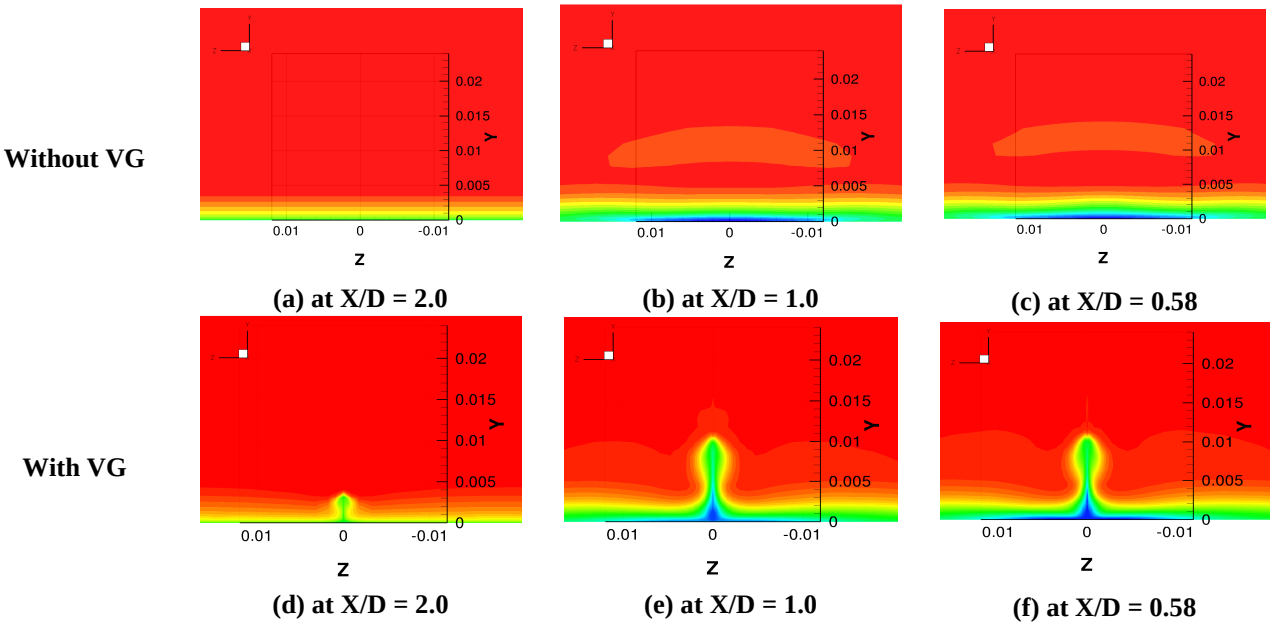

(a) at X/D = 2.0 (b) at X/D = 1.0 (c) at X/D = 0.58

(d) at X/D = 2.0 (e) at X/D = 1.0 (f) at X/D = 0.58

Figure 4: Mach Contour Upstream of Cylindrical Protrusion with and without VG.

Due to three-dimensional vortices emerging from the protrusion leads to a re-circulation zone, and flow reattachment point also depends mainly on the height of protrusion. The presence of vortex generator can help in improving the interaction zone and reduction of pressure load acting on the cylindrical protrusion. To validate the present computation, the upstream centerline pressure coefficient (C_p) for cylindrical protrusion with and without VG predicted with the code is compared with the experimental results[25] is shown in figure 2. The peak pressure acting on the cylinder and the hump region ahead of the cylinder is predicted well for cylindrical protrusion. The cylindrical protrusion height (H_C) to boundary layer thickness (δ) is 1.0. The percentage difference from the present computational results obtained is about 7% in comparison with the experimental values. The CFD results show slightly higher than experimental values. Most of the region falls within the range of error bars and predicted the trend as well.

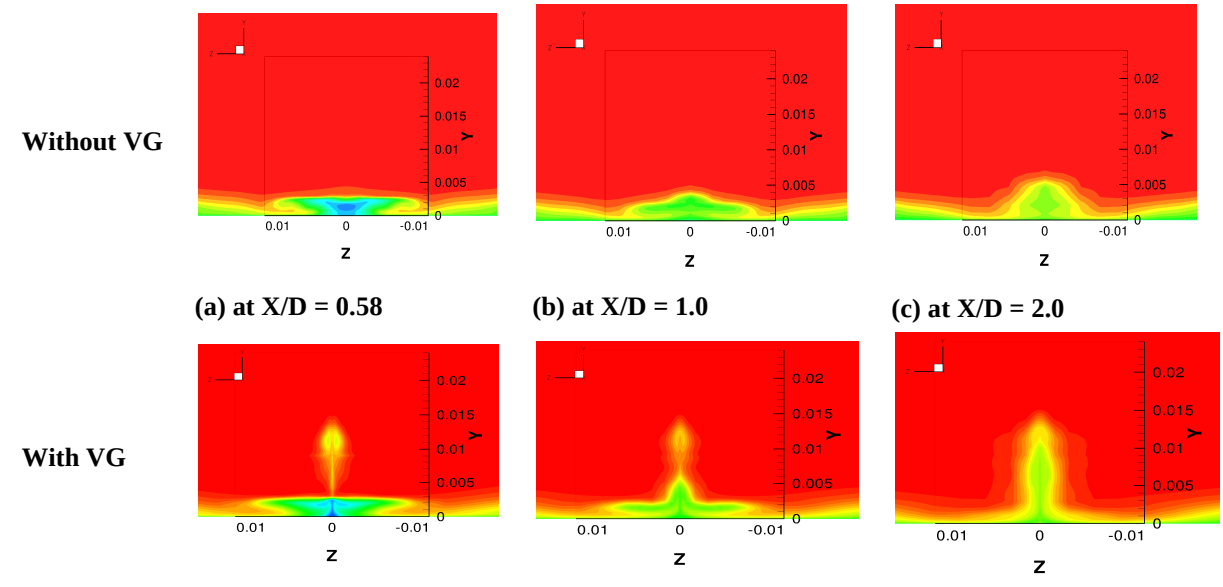

(a) at X/D = 0.58 (b) at X/D = 1.0 (c) at X/D = 2.0

(d) at X/D = 0.58 (e) at X/D = 1.0 (f) at X/D = 2.0

Figure 5: Mach Contour Downstream of Cylindrical Protrusion with and without VG.

The streamline pattern along with surface pressure contour was obtained around the cylindrical protrusion with and without VG is shown in figure 3. The streamlines pattern clearly indicates that the presence of VG can influence the primary separation line. In this study, the primary separation line is defined as the upstream extent of separated flow, or the point at which the pressure starts rising measured from the center of the cylinder. Figure 3(a) also depicts that by using a single VG, the influence is mainly along the cylindrical protrusion center line where Z/D =0. It is possible that if by adopting an array of VG can have a greater influence towards the span-wise direction but, it may add up as excrescence drag of the vehicle. Figure 3(b) shows streamline pattern on the symmetry plane (Z/D = 0). The separation region ahead of the cylindrical protrusion is clearly indicated by the circulation region upstream, and tip vortex is seen at the trailing edge of cylindrical protrusion. By placing vortex generator ahead of cylindrical protrusion, can energize the boundary layer. The reversal of streamline direction ahead of the protrusion is mainly due to the vortices in the span-wise direction. The counter rotating vortices enhance the flow around the cylindrical protrusion and mix with the vortices emanating from the protrusion. This can be seen through the stream-wise Mach contours.

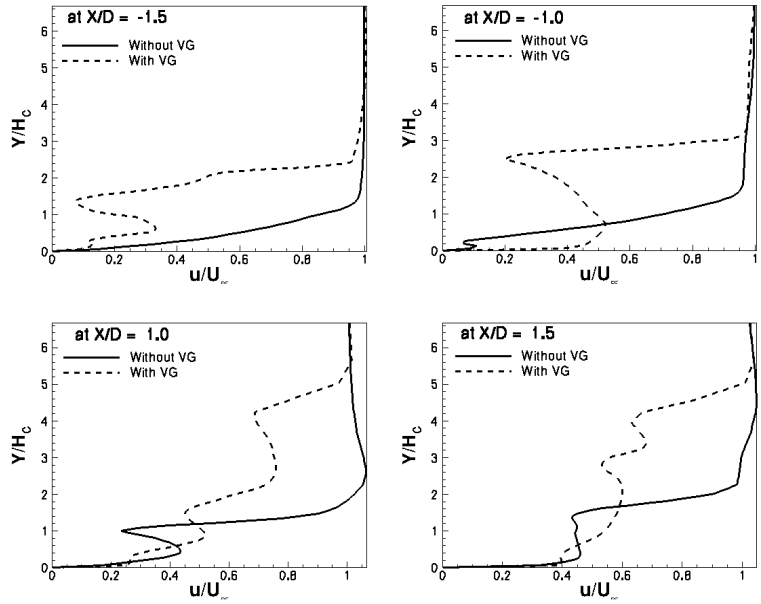

Figure 6: Velocity Profiles Plotted at Upstream and Downstream Location with and without VG (Z/D = 0).

Figure 4 shows Mach contours along the several stream wise positions ahead of the cylindrical protrusion starting from the location near downstream of VG at X/D = -0.58, -1.0, -2.0. The protrusion case without VG shows a separated region spread along the span-wise direction. The case with VG clearly indicates that the lateral (Z-direction) separation is reduced due to counter-rotating vortices. These vortices tend to increase separation along Y-direction. The downstream span-wise Mach number at X/D = 0.58, 1.0, 2.0 is shown in figure 5. The two counter-rotating vortices from the VG can able to coalesce with the horse-shoe vortices from the cylindrical protrusion. The recirculation region is also reduced by increasing the downstream pressure. In figure 6 non-dimensional velocity profile is shown at several locations upstream and downstream of cylindrical protrusion. The location at X/D = -1.5 and -1.0 is just before and after the separation zone ahead of the protrusion. In figure 6(b), the velocity profile indicates that for a case with VG shows an increase in velocity near wall region as a result of an increase in momentum transfer from a higher level to a lower level. Figure 6(c and d) shows velocity profile downstream of cylindrical protrusion at X/D = 1.0 and 1.5. It shows that the velocity near the wall region

decreases for the case with VG. This is due to the counter-rotating vortex from the VG mixes along with horseshoe vortex arising from the cylindrical protrusion. The frequency spectra of the wall pressure fluctuation upstream, downstream and on cylindrical protrusion are shown in figure 7. Figure 7(a) and (b) is plotted upstream of cylindrical protrusion at X/D = -1.0 and -1.5. The Frequency spectra show that the vortices arise from the VG can be less effective in the interaction zone. The position X/D = -1.0 falls just downstream of separation point, where -1.5 just upstream of separation point. The spectral density values show slight increased when using VG. Figure 7(c and d) shows downstream points at X/D = 1.0 and 1.5. Figure 7(e) and 7(f) shows spectral density on cylindrical protrusion leading and trailing stagnation line at Y/D = 0.5 and X/D = -0.5 and 0.5.The VG has more effect towards the downstream of the cylindrical protrusion than the upstream. The collapse of spectra is also faster in the case using VG. The less influence in the upstream might be because of weak vortices [19].

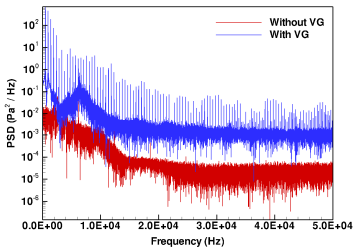

(a) at X/D = -1.0, Y/D = 0

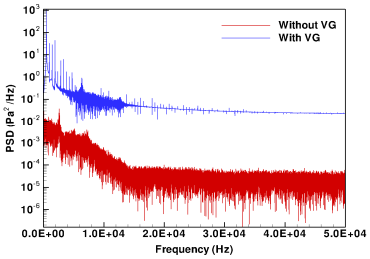

(b) at X/D = -1.5, Y/D = 0

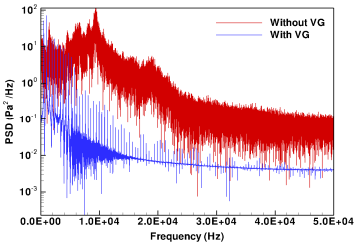

(c) at X/D = 1.0, Y/D = 0

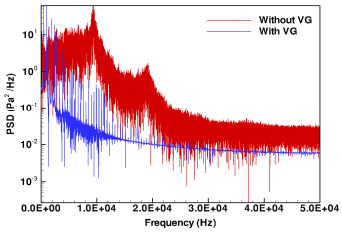

(d) at X/D = 1.5, Y/D = 0

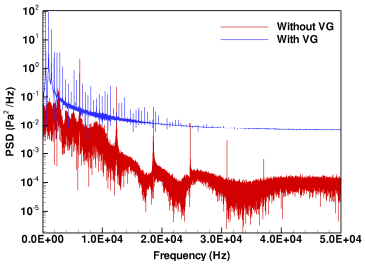

(e) at X/D = -0.5, Y/D = 0.5

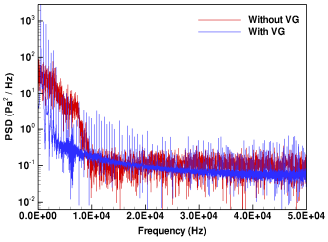

(f) at X/D = 0.5, Y/D = 0.5

Figure 7: Velocity Contour Downstream of Cylindrical Protrusion with and without VG (Upstream – a,b ; Downstream – c,d ; on Cylinder – e,f).

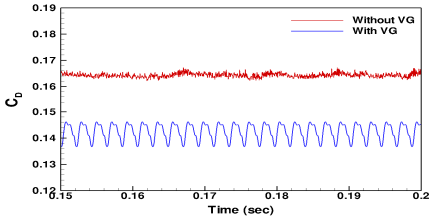

(a)

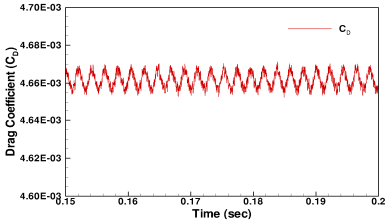

(b)

Figure 8: Coefficient of Drag Acting (a) on Cylindrical Protrusion with and without VG (b) on Vortex Generator.

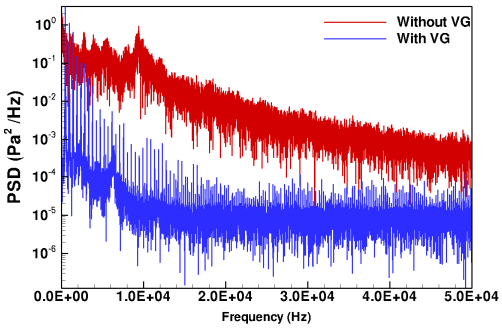

Figure 9: Coefficient of Drag Acting on VG.

The instantaneous drag coefficient shown in figure 8 clearly indicates that using a passive device like vortex generator ahead of cylindrical can be able to reduce the drag acting on that protrusion. The time averaged coefficient of drag is calculated with and without VG is 0.141 and 0.1658 respectively, which is about 15% drag reduction. Figure 9 shows the coefficient of drag due to vortex generator. The instantaneous drag coefficient due to vortex generator is obtained as 4.66E-03, which is comparatively lesser than the drag due to the cylindrical protrusion. Later, these values used to spectral analysis, which also indicating at frequency 1E+04, the spectra collapse but shows more scattering.

4. CONCLUSIONS

The unsteady effect of vortex generator on small cylindrical protrusion of height 3 mm and diameter 24 mm is investigated numerically. The present study describes the control of shock wave boundary layer interaction around the cylindrical protrusion at Mach number 2.0 and Reynolds number of 3.6e+06 /m using triangular ramp type vortex generator. Unsteady-RANS simulation is carried out along with the k-ω standard turbulence model. The counter rotating vortices arise from the VG can energize the boundary layer which helps in reduction of separation region ahead of the protrusion and also helps in reduction of pressure load acting on the cylindrical protrusion. Vortex generator can able to alleviate the shock boundary layer interaction due to the cylindrical protrusion. For the case with vortex generator, shows less spectral frequency and collapse faster than the case without VG. The aerodynamic drag acting on cylindrical protrusion can be influenced by incorporating vortex generator ahead of shock boundary layer interaction zone. The drag due to vortex generator is very small when compared to drag acting on the cylindrical protrusion and is neglected.

5. ACKNOWLEDGEMENTS

This work was supported by the National Research Foundation of Korea(NRF) grant funded by the Korea government(MSIP) (No. NRF-2016R1A2B3016436).

REFERENCES

1. *Westkaemper, J.C. (1968). Turbulent Boundary Layer Separation ahead of Cylinders. American Institute of Aeronautics and Astronautics, 6 (7), 1352-1355.*
2. *D. M. Voitenko, A. L. Zubkov, Y. A. Panov, Supersonic Gas Flow Past a Cylindrical Obstacle on a Plate, Mekhanika Zhidkosti I Gaza 1 (1966) 121-125.*
3. *R. Korkegi, Survey of Viscous Interactions Associated with High Machnumber Flight, AIAA Journal 9 (1971) 771-784.*
4. *Sedney, R.(1972). Visualization of Boundary Layer Flow patterns around Protuberances Using an Optical-Surface Indicator Technique,Physics of Fluids, 15(12), 2439- 2441.*

5. *Sedney, R. (1973). A Survey of the Effects of Small Protuberances on Boundary-Layer Flows, American Institute of Aeronautics and Astronautics, 11(6), 782- 792.*

6. *Sykes, D.M. (1962). The Supersonic and Low-Speed Flows Past Circular Cylinders of Finite Length Supported at One End, Journal of Fluid Mechanics, 12(3), 367- 387.*

7. *Sedney, R., and Kitchens, C.W. (1977). Separation ahead of Protuberances in Supersonic Turbulent Boundary Layers, American Institute of Aeronautics and Astronautics, 15(4), 546- 552.*

8. *Mashburn, J. H. (1969). Turbulent Boundary Layer Separation Ahead of Cylindrical Protuberances in Supersonic Flow, ARL-TR-69-17.*

9. *Verma, S. B. and Gupta, V. (1995). Supersonic Separation with Obstructions, American Institute of Aeronautics and Astronautics,34(4), 849 – 850.*

10. *Majid, M. and David W. F. (2009). Thermal Response of Supersonic Airflow to a Fin Protrusion Situated on a Curved Surface, Journal of Heat Transfer, ASME Journal, 131(11).*

11. *Mandal, S. K., SEN, D., & GIRI, A. (2018). Multi objective optimization of laminar mixed convective heat transfer of electronic chips in a horizontal channel with vortex generator. International Journal of Mechanical and Production Engineering Research and Development, 8, 155-166.*

12. *Yu, M. S., Song, J., Bae, J. C., and Cho, H. H. (2012). Heat transfer by shock wave/boundary layer interaction on a flat surface with a mounted cylinder, International journal of Heat and Mass Transfer, Vol 55, 2012, pp. 1764-1772.*

13. *Li, S., Shi, Y., and Chen, Y. (1995). The Effects of the Short Protuberance on Interactive Flowfield at Hypersonic Speed, AIAA Paper 95-1829-CP, 13th AIAA Applied Aerodynamics conference.*

14. *Hahn, P. V., and Frendi, A. (2013). Interaction of three-dimensional protuberances with a supersonic Turbulent Boundary layer, American Institute of Aeronautics and Astronautics,51(7), 1657-1666.*

15. *Z.R. Murphree, J. Jagodzinski, E.S. Hood, Jr., N.T. Clemens, and D.S. Dolling (2006). Experimental Studies of Transitional Boundary Layer Shock Wave Interactions, AIAA 2006-326.*

16. *Babinsky, H. and Ogawa, H. (2008). SBLI control for wings and inlets, Shockwaves 18(2), 89-96.*

17. *Lin, J. C. (2002). Review of Research on Low-Profile Vortex Generators to Control Boundary-Layer Separation, Progress in Aerospace Sciences, 4–5(38), 389–420.*

18. *JHA, B. M., & Mandal, A. (2016). Overcut and Profile of the Machined Features in Electrochemical Machining. IASET: IJMMCE, 1(1), 29*

19. *Lu, F. K., Li, Q., Shih, Y., Pierce, A. J., and Liu, C. (2011). Review of Micro Vortex Generators in High-Speed Flow, AIAA Paper 2011-31.*

20. *Loth, E., and Lee, S. (2008). Understanding Micro-Ramp Control for Shock Boundary Layer Interactions, US Air Force Research lab., Rept. AFRL-SR-AR-TR-08-0145.*

21. *S. Lee, Large Eddy Simulation of Supersonic Boundary Layer Interaction Control Using Micro-Vortex Generator, PhD Thesis, University of Illinois, 2009.*

22. *Babinsky, H., (2008). Understanding Micro-Ramp control for Shock Boundary Layer Interaction, US Air Force Research Lab., Rept. AFRL-SR-AR-TR-08-0074.*

23. *Babinsky, H., Li, Y., and Pitt Ford, C. W. (2009). Micro ramp Control of Supersonic Oblique Shock Wave/Boundary Layer*

Interactions, American Institute of Aeronautics and Astronautics, 47(3), 6–13.

24. *B. H. Anderson, J. Tinapple, L. Surber, (2006).Optimal Control of Shock Wave Turbulent Boundary Layer Interactions Using Micro-Array Actuation, AIAA Paper 2006-3197.*
25. *S. Hirt, B. H. Anderson, Experimental Investigation of the Application of Micro ramp Flow Control to an Oblique Shock Interaction", AIAAPaper 2009-919 (2009).*
26. *T. Herges, E. Kroeker, G. Elliott, C. Dutton, Microramp Flow Control of Normal Shock/Boundary-Layer Interactions", AIAA Journal 48 (2010) 2529-2542.*
27. *Rybalko, M., Loth, E., Chima, R., Hirt, S., and Debonis, J., (2009). Micro-Ramps for External Compression Low-Boom Inlets, AIAA Paper 2009-4206.*
28. *Rybalko, M., and Loth, E., (2015). Aerodynamic Impact of Vortex Generators on a Relaxed-Compression Low Boom Inlet, American Institute of Aeronautics and Astronautics,53(12), 3700–3712.*
29. *Khan, S. A., Ullah, M. A., Ahmed, G. F., Jalaluddin, A., & Baig, M. A. A. (2018). Flow control with aero-spike behind bluff body. Int. J. Mech. Prod. Eng. Res. Dev.(IIJMPERED), 8(3), 1001-1008.*
30. *HoldenH., and Babinsky H., Effects of Microvortex Generators on Separated Normal Shock/ Boundary Layer Interactions", Journal of Aircraft 44 (2007) 170-174.*
31. *M. Galbraith, P. Orkwis, J. Benek, Multi-Row Micro-Ramp Actuators for Shock Wave Boundary Layer Interaction control", AIAA Paper 2009-321 (2009).*
32. *J. Barter, D. Dolling, Reduction of Fluctuating Pressure Loads in Shock/Boundary Layer Interaction Using Vortex Generators", AIAA Journal 33 (1995) 1842-1849.*
33. *Pierce, A. J., Li, Q., Shih, Y., Lu, F. K., and Liu, C. (2011). Interaction of Micro-vortex Generator Flow with Ramp Induced Shock Boundary Layer Interactions, AIAA Paper 2011-32.*
34. *Vignesh Ram, P.S., T.Setoguchi and H.D. Kim, (2016). Effects of Vortex generator on Cylindrical Protrusion Aerodynamics, Journal of Thermal Science, 25(1), 7–12.*
35. *Vignesh Ram, P.S., S. Das., and H. D. Kim. (2016). Influence of vortex generator on cylindrical protrusion aerodynamics at various Mach numbers, Journal of Aerospace Science and Technology, 58, 267-274.*
36. *Vignesh Ram, P.S., (2011). Flow Field Investigation around Cylindrical Protrusion with Vortex Generator", Master Thesis, BIT Mesra, India.*

AUTHOR'S PROFILE

Vignesh Ram Petha Sethuraman received his M.E degree in Space Engineering and Rocketry from Birla Institute of Technology, Mesra, India in 2011. He is presently Ph.D. research scholar at Andong National University, South Korea. His research interests include rarefied gas dynamics, computational fluid dynamics, Shock boundary layer interactions, monte-carlo simulations.

Heuy-Dong Kim received his B.S. and M.S. Degrees in Mechanical Engineering from Kyungpook National University, Korea, in 1986 and 1988, respectively. He then received his Ph. D. From Kyushu University, Japan, in 1991. Dr. Kim is currently a Professor at the School of Mechanical Engineering, Andong National University, Korea. Professor Kim is interested in the research areas related to compressible flows including shock wave turbulent boundary layer interactions, unsteady internal flows, and shock tube & supersonic wind tunnel technologies. He studies compressible flow physics using both the computational fluid dynamics and experiment. He also develops new technologies on the fluid machinery of high-speed flows. The medical applications of shock wave and the supercritical fluid dyeing process of textiles are primary subjects of his recent research.